IJFANS INTERNATIONAL JOURNAL OF FOOD AND NUTRITIONAL SCIENCES
ISSN PRINT 2319 1775 Online 2320 7876
Research paper
 UGC CARE Listed (Group -I) Journal Volume 11, Iss 11, 2022

Charge Transport Properties of ZnO Doped PPY Composite Samples

Promila Jangra, Vikram Singh

Dept of Physics, OSGU, Hisar

promilajangra82@gmail.com

vikramdobal@gmail.com

Corresponding Author Email; promilajangra82@gmail.com

Abstract

In the present research work, pristine and ZnO nanoparticles doped polypyrrole-based samples were synthesized using a simple chemistry-based polymerization process using three different doping concentrations of ZnO. The prepared samples were characterized using various techniques. X-ray diffraction spectra of prepared samples indicate that these samples are quasi-crystals in nature. Fourier transformation infrared spectroscopy of these samples contains the various required fundamental bands which confirms the synthesis of expected samples. Field emission scanning electron microscopy of synthesized samples reveals that these samples have particle-like morphology. The thermal properties of prepared samples were investigated using the thermal gravimetric analysis investigation. Moreover, the electrical properties of prepared samples were investigated in the temperature range 293 to 393 K. The conductivity of prepared samples increases with the increase in temperature which indicates the semi-conducting nature of prepared samples.

Keywords: PPY; ZnO; TGA; Semi-conductor; Mott's Hopping.

ISSN PRINT 2319 1775 Online 2320 7876
Research paper UGC CARE Listed (Group -I) Journal Volume 11, Iss 11, 2022

Introduction

In literature, insulators make up the majority of the described polymers. Later research however demonstrated that polymers can also behave in a semiconducting material. Polymers have potential uses in many different disciplines because they have special optical, electrical, and thermal properties. In addition to other conducting polymers, polypyrrole (PPY) has received a great deal of attention because of its non-redox doping, strong thermal and environmental stability, high conductivity, and practicality. The characteristics of PPY alter dramatically in composite form. Such composites have been demonstrated for use in applications such as polymeric batteries, shielding at the electromagnetic/radio frequency interface in electronic devices, such as the plastic housing of computers and cell phones, temperature and current sensor devices, and electrochromic displays. Metal oxides (MOs) can be mixed with PPY to further enhance its processability, mechanical attributes, and conductivity. Because it is difficult to achieve chemical interactions between PPY and MOs, making PPY-MO composites is tough. Because of their increased qualities and prospective uses in a variety of disciplines, researchers continue to concentrate on synthesizing PPY and MO composites using diverse approaches [1]. Until now, conducting polymers have been used as a shell to enclose inorganic nanoparticles like ZnO, creating a variety of nanocomposites [2]. PPY/ZnO nanocomposite was created by Xia and Wang [3] using ultrasonic irradiation. Using the sol-gel method, Schnitzler and Zarbin [4] produced hybrid materials including PPY and ZnO nanoparticles. The most popular cathode candidates in the advancement of lithium and lithium-ion battery technology are transition-metal oxides [5].

ISSN PRINT 2319 1775 Online 2320 7876
Research paper UGC CARE Listed (Group -I) Journal Volume 11, Iss 11, 2022

Other crystalline oxides, such as V_2O_5, MnO_2, MoO_3, and WO_3, have also been employed as cathodes in solar cells [6,7] and rechargeable lithium batteries [8,9]. Additionally, PPY filled with materials such as magnetic particles [10-12], dielectric particles [13-17], or carbonaceous fillers [18-20], exhibit a combination of dielectric/magnetic and electrical properties. Applications for these composites in the fields of microwave absorption [20], supercapacitors [21], and corrosion control [22], among others, have been proven. PPY/NiO nanoparticle, a nanobelt, and a nanotube were created by chemically synthesizing PPY and NiO composites by Song and colleagues in the presence of sodium dodecyl benzene sulfonate. The thermostability and conductivity of the composite materials improved [23–25].

Although several investigations on PPY/ZnO composites have been described, most researchers are still concentrating on their synthesis and characterization. To the author's knowledge, there isn't any publication on the analysis of dynamical parameters for PPY/ZnO composites using methods like TGA, though. Therefore, a thorough investigation employing various ZnO concentrations in PPY and methodologies is required.

Experimental Details

Sample Preparation

The pristine PPY and PPY/ZnO composite samples were prepared using the chemical oxidative polymerization synthesis process. In order to do this, two different aqueous solutions of pyrrole and ferric chloride were prepared separately in the molar concentration 1 M and 1.25 M. The prepared solutions were then cooled in a refrigerator for 2 hrs. Thereafter, the monomer solution was kept in an ice bath maintaining the

ISSN PRINT 2319 1775 Online 2320 7876
Research paper
 UGC CARE Listed (Group -I) Journal Volume 11, Iss 11, 2022

temperature between 0 to 4 ^{o}C. Then, the oxidant solution is added dropwise in the monomer solution, then the polymerization reaction starts quickly, and allow to react for 24 hrs. After the appropriate time, the obtained solution starts to filtrate using filter paper, and obtained yield was washed with 1 M HCl and then with acetone till the filtrate become colorless. Then, this yield was firstly air dried and then in vacuum. Using, the pestle mortars this dried sample was crushed in fine powder. The similarly synthesis route followed for 5, 10 and 15 wt% ZnO doped PPY composite samples.

Experimental Techniques

Rigaku Miniflex-II diffractometer was used to record XRD patterns with CuK_{α} in the angle of 2θ (10-80^{o}) at a slow scanning rate of 2^{o}/min. Data from X-ray diffraction (XRD) was used to establish the samples' crystal structure. The powder sample was mixed with dry KBr in a ratio of 1:20 by weight for the FTIR analysis using a Shimadzu IR affinity-1 8000 FTIR spectrophotometer. Using the scanning electron microscope EVO 18, the surface's microstructure was examined. By using a TA instrument with the model number SDT Q600 and a heating rate of 10 ^{o}C/min in a nitrogen atmosphere, thermogravimetric analysis was carried out. The Keithley 6517B electrometer was used to test DC conductivity at 1V and temperatures ranging from 25 to 120 ^{o}C with a variation of 2 ^{o}C.

Results and Discussion

X-ray Diffraction (XRD) Analysis

Figure 1 displays the XRD patterns of pure PPY and PPY/ZnO composites. The XRD pattern of PPY and PPY/ZnO composite samples contain the two identical peaks

ISSN PRINT 2319 1775 Online 2320 7876
Research paper
 UGC CARE Listed (Group -I) Journal Volume 11, Iss 11, 2022

around ~21.44 and 26.12^{o} whereas a soldier around ~16.10^{o}. The intensity of peaks significantly changes with introducing the ZnO nanoparticles in PPY symmetry which indicates the strong interaction between PPY and ZnO. These two beaks are present due to quinoid and benzenoid rings in the parallel and perpendicular directions. Moreover, the presence of these two peaks indicates that the prepared samples exhibit structure of quasi-crystals.

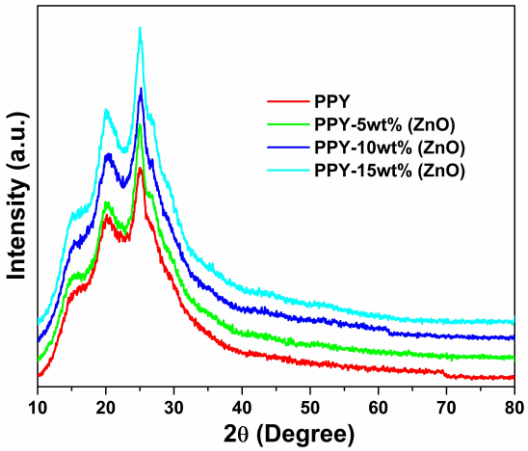

Figure 1: XRD patterns of PPY and PPY/ZnO composites.

Fourier Transform Infrared (FTIR) Analysis

FTIR spectra of pristine and ZnO-doped PPY composite samples are shown in Figure 2. FTIR spectrum reveals distinctive vibrations between 400 and 2000 cm-1. At 518, 813, 1159, 1321, 1493, and 1591 cm^{-1}, it exhibits unique bands. The bands at 518 and 813 cm^{-1} are caused by para-disubstituted aromatic rings and C-H out-of-plane bending vibration, respectively. The C-N stretching vibrations are represented by a band that may be seen near 1321 cm^{-1}. At 1159 cm^{-1}, vibration in C-H occurs when the plane is bent [26]. Non-symmetric C6 ring stretching modes are thought to be the cause of the bands that are present in the 1450-1600 cm^{-1} range [27]. The quinoid rings play a

ISSN PRINT 2319 1775 Online 2320 7876
Research paper
 UGC CARE Listed (Group -I) Journal Volume 11, Iss 11, 2022

significant role in the higher frequency vibration at 1591 cm^{-1}, while the benzenoid ring units may be seen in the lower frequency mode at 1493 cm^{-1}. While the band seen in the range 2950-3300 cm^{-1} is attributable to N-H stretching of aromatic amines, the peak detected at 2300 cm^{-1} is due to aromatic C-H stretching vibrations [28-30].

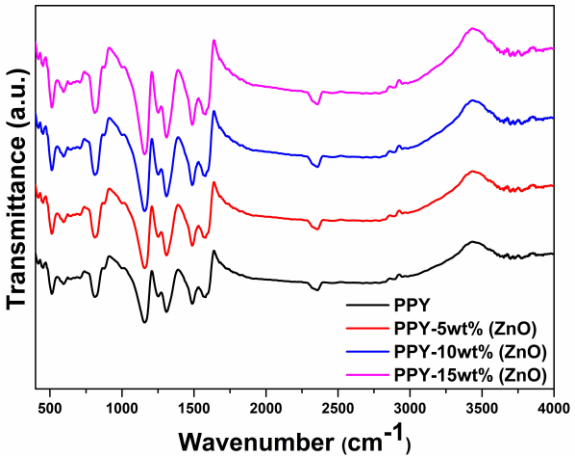

Figure 2: FTIR spectra of PPY and PPY/ZnO composites

Field Emission Scanning Electron Microscopy (FESEM)

Figure 3(a-d) displays typical FESEM images for pure PPY and PPY/ZnO composite samples. FESEM images of presently prepared samples indicates that these samples have particles like morphology for pristine and ZnO doped PPY samples. In the FESEM images of composite samples, no ZnO nanoparticles are observed which may be due to incorporation of ZnO nanoparticles in PPY matrix. Here, ZnO nanoparticles behave as core whereas PPY as shell [31].

ISSN PRINT 2319 1775 Online 2320 7876
Research paper
 UGC CARE Listed (Group -I) Journal Volume 11, Iss 11, 2022

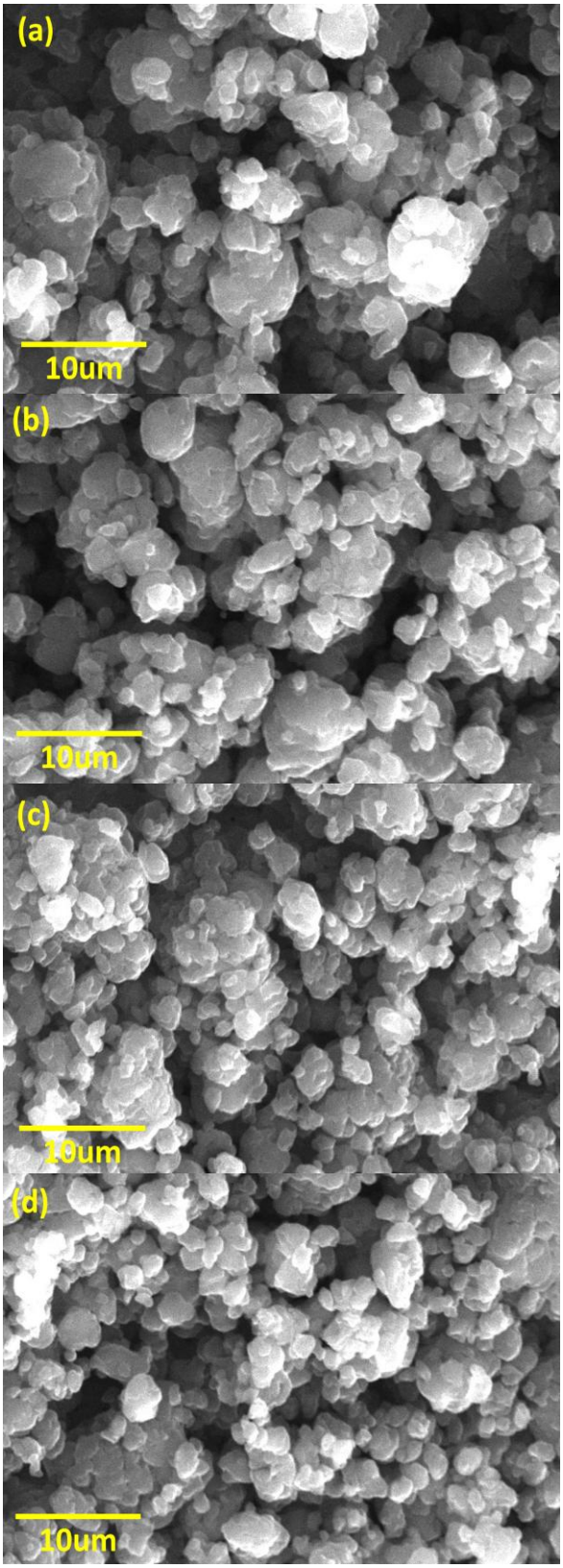

ISSN PRINT 2319 1775 Online 2320 7876
Research paper
 UGC CARE Listed (Group -I) Journal Volume 11, Iss 11, 2022

Figure 3: FESEM images of PPY and PPY/ZnO composites

Thermogravimetric Analysis (TGA)

Figure 4 displays TGA thermograms of PPY and PPY/ZnO composites in a nitrogen atmosphere. The four processes of weight reduction are revealed by the TGA analysis of PPY and PPY/ZnO composites.

1. The initial dehydration stage is thought to begin at around 100 ^{o}C and is caused by the desorption of water that has been absorbed at the surface of the doped polymer [32].

2. The elimination of the protonic acid component causes the second stage to occur at around 250 ^{o}C [32].

3. The third at roughly ~510 °C and the fourth at roughly ~640 °C indicate the break in the polymer chain, which may result in the formation of gases [33].

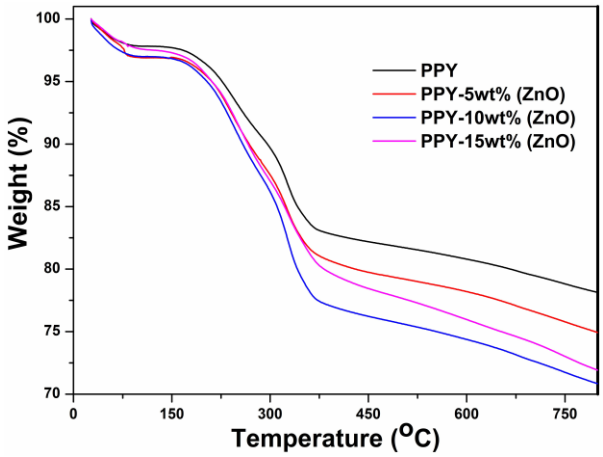

Figure 4: TGA thermograms of PPY and PPY/ZnO composites

Current-Voltage (I-V) Characteristics (DC Conductivity)

Conducting polymers' conduction mechanisms differ significantly from those of intrinsic semiconductors in that the current does not grow linearly with applied voltage

ISSN PRINT 2319 1775 Online 2320 7876
Research paper
 UGC CARE Listed (Group -I) Journal Volume 11, Iss 11, 2022

[34-36]. In conducting polymers, the initial addition of negative and positive charges does not immediately cause the stiff conduction or valence bands to start to fill. Permanent dipoles are absent in conductive polymers. In actuality, the sample contains random charge (polaron) trapping sites. Strong coupling between electrons and phonons results in lattice distortions around the doped charge when an external field is applied. As a result, charge trapping becomes strong, and their localized motion acts as an efficient electric dipole. As a result, quasiparticles like polarons and bipolarons are created. These polarons and bipolarons are used in this instance to carry a charge. The generation of polarons and bipolarons rises with the increasing applied field, which helps accelerate the current increase with respect to voltage and produce a nonlinear curve [37]. The electrical properties of prepared samples were investigated in the temperature range 293 to 393 K. Figures 5(a,b) indicates the variation in electrical conductivity with the increase in temperature.

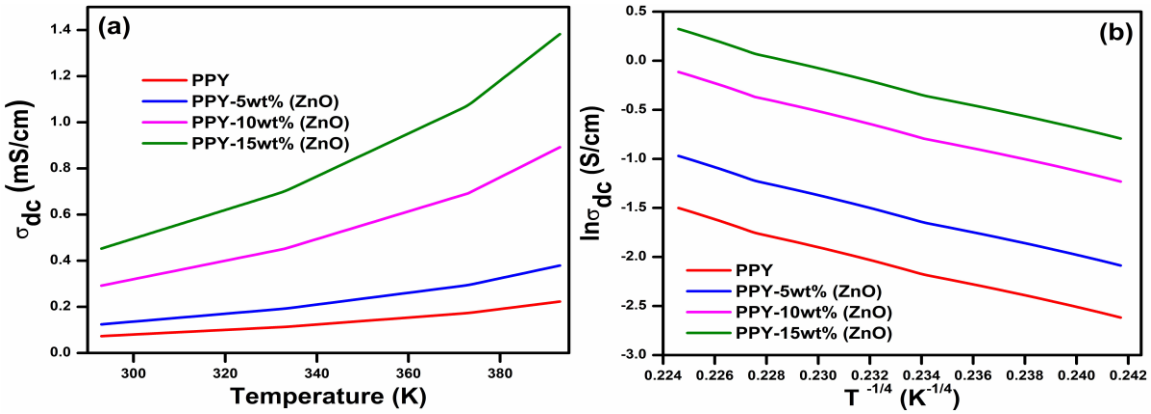

Figure 5: I-V characteristics of (a) PPY (b) t20 (c) t40 (d) t50 at different temperatures

Equation (1), which is provided as, has been used to estimate the values of dc electrical conductivities (dc) at various temperatures at 1V based on the recorded I-V characteristics of these samples [38-40].

ISSN PRINT 2319 1775 Online 2320 7876
Research paper
 UGC CARE Listed (Group -I) Journal Volume 11, Iss 11, 2022

$$\sigma_{dc} = \frac{I\ x\ L}{V\ x\ A} \quad (1)$$

Where L and A stand for the sample's thickness and area, respectively, and V stands for voltage. Figure 5a also displays the fluctuation of dc conductivity with temperature for PPY and PPY/ZnO composites. All of the samples' DC conductivity (dc) measurements were found to follow the Arrhenius relation as described in equation 2, which is [41-44]

$$\sigma_{dc}(T) = \sigma_0\ \exp\left(\frac{-W}{kT}\right) \quad (2)$$

Where σ_0 is the pre-exponential parameter which depends on semiconductor nature, W denotes the thermal activation energy of electrical conduction, and k is Boltzmann's constant.

The slope of the curve ln(dc) vs 1/T can be used to compute the values of the activation energy owing to electrical conduction using equation 2. For each sample, the slope is determined via linear fitting, and these samples having values of activation energy 6.26, 5.73, 5.33, 4.91 meV for pristine PPY and 5, 10 and 15 wt% ZnO doped PPY samples, respectively. According to these values of activation energy, it is observed that the activation energy values decrease with the increase in doping concentration which indicates the lower energy required for charge transport mechanism [45-47].

Figure 5b illustrates the plot of $\ln\sigma_{dc}$ vs. $T^{-1/4}$, which similarly has a very strong linear fitting (with linearity 0.99), and shows that all of the samples exhibit three-dimensional (3D) charge transport, which is previously explained by equation (3) [48-50].

$$\sigma_{dc} = \sigma_0 e^{-\left(\frac{T_0}{T}\right)^{\gamma}} \quad (3)$$

ISSN PRINT 2319 1775 Online 2320 7876

 UGC CARE Listed (Group -I) Journal Volume 11, Iss 11, 2022

Where T_o is the Mott's characteristic temperature related to the degree of localization of the electronic wave function. The dimensionality of the conducting media is determined by the exponent = 1/(1+d). For the purpose of understanding the variable range hopping (VRH) of disordered materials in the low temperature region, the Mott's model was presented. However, this model works well for explaining dc conductivity data at high temperatures for the composites that are now available [51-53].

Conclusions

PPY and ZnO-doped PPY composite samples were prepared using the chemical oxidative polymerization synthesis route. The presence of highly conducting state peaks of benzenoid and quinoid rings in the FTIR spectra of prepared samples indicates the prepared samples are in emeraldine salt form of PPY-based pristine and composite samples. XRD pattern of presently prepared samples indicates the quasi-crystal nature of prepared samples. TGA indicates that the pristine as well as doped samples exhibit their more than 70% weight even after 800 ^{o}C temperature. This indicates that the stability of prepared samples increases with the increase in ZnO nanoparticle doping concentration. The FESEM images of prepared samples indicate that the prepared samples have a particle size in the range of 2 to 10 um. The prepared samples follow Mott's variable hopping model for the charge transport mechanism.

REFERENCES

1. Gangopadhyay, R., & De, A. (2000). Conducting polymer nanocomposites: a brief overview. *Chemistry of materials*, *12*(3), 608-622.L. J. Zang and M. X. Wang, *J. Phys. Chem.* **107** (2003) 6748.

ISSN PRINT 2319 1775 Online 2320 7876
Research paper
 UGC CARE Listed (Group -I) Journal Volume 11, Iss 11, 2022

2. Xia, H., & Wang, Q. (2002). Ultrasonic irradiation: a novel approach to prepare conductive polyaniline/nanocrystalline titanium oxide composites. *Chemistry of Materials*, *14*(5), 2158-2165.

3. Schnitzler, D. C., & Zarbin, A. J. (2004). Organic/inorganic hybrid materials formed from TiO2 nanoparticles and polyaniline. *Journal of the Brazilian Chemical Society*, *15*, 378-384.

4. Peng, Z. S., Wan, C. R., & Jiang, C. Y. (1998). Synthesis by sol–gel process and characterization of LiCoO2 cathode materials. *Journal of Power Sources*, *72*(2), 215-220.

5. Sethi, N., Bhardwaj, P., Kumar, S., & Dilbaghi, N. (2019). Development and Evaluation of Ursolic Acid Co-Delivered Tamoxifen Loaded Dammar Gum Nanoparticles to Combat Cancer. *Advanced Science, Engineering and Medicine*, *11*(11), 1115-1124.

6. Gemeay, A. H., Nishiyama, H., Kuwabata, S., & Yoneyama, H. (1995). Chemical preparation of manganese dioxide/polypyrrole composites and their use as cathode active materials for rechargeable lithium batteries. *Journal of the Electrochemical Society*, *142*(12), 4190..

7. Wang, J. B., Huang, G. J., Zhong, X. L., Sun, L. Z., Zhou, Y. C., & Liu, E. H. (2006). Erratum:"Raman scattering and high temperature ferromagnetism of Mn-doped ZnO nanoparticles"[Appl. Phys. Lett. 88, 252502 (2006)]. *Applied Physics Letters*, *89*(5).

ISSN PRINT 2319 1775 Online 2320 7876
Research paper
 UGC CARE Listed (Group -I) Journal Volume 11, Iss 11, 2022

8. Shrotriya, V., Li, G., Yao, Y., Chu, C. W., & Yang, Y. (2006). Transition metal oxides as the buffer layer for polymer photovoltaic cells. *Applied Physics Letters*, *88*(7)..

9. Saini, P., Choudhary, V., Vijayan, N., & Kotnala, R. K. (2012). Improved electromagnetic interference shielding response of poly (aniline)-coated fabrics containing dielectric and magnetic nanoparticles. *The Journal of Physical Chemistry C*, *116*(24), 13403-13412..

10. Zhang, B., Du, Y., Zhang, P., Zhao, H., Kang, L., Han, X., & Xu, P. (2013). Microwave absorption enhancement of Fe3O4/polyaniline core/shell hybrid microspheres with controlled shell thickness. *Journal of Applied Polymer Science*, *130*(3), 1909-1916.

11. Abbas, S. M., Chatterjee, R., Dixit, A. K., Kumar, A. V. R., & Goel, T. C. (2007). Electromagnetic and microwave absorption properties of (Co2+–Si4+) substituted barium hexaferrites and its polymer composite. *Journal of applied physics*, *101*(7).

12. Jumali, M. H., Izzuddin, I., Ramli, N., Salleh, M., & Yahaya, M. (2009). Comparative studies on microstructural and gas sensing performance of TiO2 and TiO2-PANi nanocomposite thin films. *Solid State Sci. Technol*, *17*, 126-131..

13. Saini, P., Arora, M., Gupta, G., Gupta, B. K., Singh, V. N., & Choudhary, V. (2013). High permittivity polyaniline–barium titanate nanocomposites with excellent electromagnetic interference shielding response. *Nanoscale*, *5*(10), 4330-4336..

14. Sethi, N., Bhardwaj, P., Kumar, S., & Dilbaghi, N. (2019). Development and Evaluation of Ursolic Acid Loaded Eudragit-E Nanocarrier For Cancer Therapy. *International Journal Of Pharmaceutical Research (09752366)*, *11*(2).

15. Pawar, S. G., Patil, S. L., Chougule, M. A., Raut, B. T., Jundale, D. M., & Patil, V. B. (2010). Polyaniline: TiO2 nanocomposites: Synthesis and characterization. *Arch. Appl. Sci. Res*, *2*(2), 194-201..

16. Dey, A., De, S., De, A., & De, S. K. (2004). Characterization and dielectric properties of polyaniline–TiO2 nanocomposites. *Nanotechnology*, *15*(9), 1277..

17. Maiti, S., Shrivastava, N. K., Suin, S., & Khatua, B. B. (2013). Polystyrene/MWCNT/graphite nanoplate nanocomposites: efficient electromagnetic interference shielding material through graphite nanoplate–MWCNT–graphite nanoplate networking. *ACS Applied Materials & Interfaces*, *5*(11), 4712-4724..

18. Saini, P., & Choudhary, V. (2013). Enhanced electromagnetic interference shielding effectiveness of polyaniline functionalized carbon nanotubes filled polystyrene composites. *Journal of nanoparticle research*, *15*, 1-7.

19. Saini, P., Choudhary, V., Singh, B. P., Mathur, R. B., & Dhawan, S. K. (2011). Enhanced microwave absorption behavior of polyaniline-CNT/polystyrene blend in 12.4–18.0 GHz range. *Synthetic Metals*, *161*(15-16), 1522-1526..

20. Caggiani, M. C., Cosentino, A., & Mangone, A. (2016). Pigments Checker version 3.0, a handy set for conservation scientists: A free online Raman spectra database. *Microchemical Journal*, *129*, 123-132..

ISSN PRINT 2319 1775 Online 2320 7876

 UGC CARE Listed (Group -I) Journal Volume 11, Iss 11, 2022

21. Jeyaprabha, C., Sathiyanarayanan, S., & Venkatachari, G. (2006). Polyaniline as corrosion inhibitor for iron in acid solutions. *Journal of applied polymer science*, *101*(4), 2144-2153..

22. Song, G., Bo, J., & Guo, R. (2005). Synthesis of the composite material of polyaniline/NiO/sodium dodecylbenzenesulfonate in micelles. *Colloid and Polymer Science*, *283*, 677-680.

23. Song, G., Han, J., & Guo, R. (2007). Synthesis of polyaniline/NiO nanobelts by a self-assembly process. *Synthetic Metals*, *157*(4-5), 170-175.

24. Han, J., Song, G., & Guo, R. (2006). Synthesis of rectangular tubes of polyaniline/NiO composites. *Journal of Polymer Science Part A: Polymer Chemistry*, *44*(13), 4229-4234..

25. Su, S. J., & Kuramoto, N. (2000). Processable polyaniline–titanium dioxide nanocomposites: effect of titanium dioxide on the conductivity. *Synthetic metals*, *114*(2), 147-153.

26. O'regan, B., & Grätzel, M. (1991). A low-cost, high-efficiency solar cell based on dye-sensitized colloidal TiO2 films. *nature*, *353*(6346), 737-740..

27. Oey, C. C., Djurišić, A. B., Wang, H., Man, K. K. Y., Chan, W. K., Xie, M. H., ... & Chui, P. C. (2006). Polymer–TiO2 solar cells: TiO2 interconnected network for improved cell performance. *Nanotechnology*, *17*(3), 706..

28. Raghavendra, S. C., Khasim, S., Revanasiddappa, M., Ambika Prasad, M. V. N., & Kulkarni, A. B. (2003). Synthesis, characterization and low frequency ac conduction of polyaniline/fly ash composites. *Bulletin of Materials Science*, *26*, 733-739.

ISSN PRINT 2319 1775 Online 2320 7876

 UGC CARE Listed (Group -I) Journal Volume 11, Iss 11, 2022

29. Vishnuvardhan, T. K., Kulkarni, V. R., Basavaraja, C., & Raghavendra, S. C. (2006). Synthesis, characterization and ac conductivity of polypyrrole/Y 2 O 3 composites. *Bulletin of Materials Science*, *29*, 77-83.

30. Klug, H. P., & Alexander, L. E. (1974). *X-ray diffraction procedures: for polycrystalline and amorphous materials* (p. 992).

31. Chen, S. A., Chuang, K. R., Chao, C. I., & Lee, H. T. (1996). White-light emission from electroluminescence diode with polyaniline as the emitting layer. *Synthetic Metals*, *82*(3), 207-210.

32. Vivek, V., Sethi, N., & Kaura, S. (2022). Green synthesis and evaluation of antibacterial activity of zinc nanoparticles from Calotropis procera leaves..

33. Goyal, S. L., Sharma, S., Jain, D., & Kishore, N. (2015). Study of structural, electrical and thermal properties of polyaniline/ZnO composites synthesized by in-situ polymerization. *Indian Journal of Pure & Applied Physics (IJPAP)*, *53*(7), 456-463.

34. Koronkiewicz, B. M. (2020). *Distance and Thermodynamic Effects in Proton Coupled Electron Transfer Model Systems* (Doctoral dissertation, Yale University)..

35. Gupta, R., Kumar, V., Goyal, P. K., Goyal, S. L., Kandwal, P., Mohapatra, P. K., & Rajeswari, B. (2011). Effect of γ-irradiation on thermal stability of CR-39 polymer. *Adv. Appl. Sci. Res.*, *2*, 248-254..

36. Reghu, M., Cao, Y., Moses, D., & Heeger, A. J. (1993). Counterion-induced processibility of polyaniline: Transport at the metal-insulator boundary. *Physical Review B*, *47*(4), 1758.

37. Earle, M. D. (1942). The electrical conductivity of titanium dioxide. *Physical Review*, *61*(1-2), 56..

38. Machappa, T., & Prasad, M. A. (2009). AC conductivity and dielectric behavior of polyaniline/sodium metavenadate (PANI/NaVO3) composites. *Physica B: Condensed Matter*, *404*(21), 4168-4172.

39. Anilkumar, K. R., Parveen, A., Badiger, G. R., & Prasad, M. A. (2009). Effect of molybdenum trioxide (MoO3) on the electrical conductivity of polyaniline. *Physica B: Condensed Matter*, *404*(12-13), 1664-1667..

40. Patil, R., Roy, A. S., Anilkumar, K. R., Jadhav, K. M., & Ekhelikar, S. (2012). Dielectric relaxation and ac conductivity of polyaniline–zinc ferrite composite. *Composites Part B: Engineering*, *43*(8), 3406-3411..

41. Ozkazanc, E., Zor, S., & Ozkazanc, H. (2012). Synthesis, characterization, and AC conductivity of polyaniline/selenium composites. *Journal of Macromolecular Science, Part B*, *51*(11), 2122-2132..

42. Kaura, S., Parle, M., Insa, R., Yadav, B. S., & Sethi, N. (2022). Neuroprotective effect of goat milk. *Small Ruminant Research*, *214*, 106748..

43. Belin, R., Zerouale, A., Pradel, A., & Ribes, M. (2001). Ion dynamics in the argyrodite compound Ag7GeSe5I: non-Arrhenius behavior and complete conductivity spectra. *Solid State Ionics*, *143*(3-4), 445-455.

44. Punia, R., Kundu, R. S., Dult, M., Murugavel, S., & Kishore, N. (2012). Temperature and frequency dependent conductivity of bismuth zinc vanadate semiconducting glassy system. *Journal of Applied Physics*, *112*(8)..

ISSN PRINT 2319 1775 Online 2320 7876

 UGC CARE Listed (Group -I) Journal Volume 11, Iss 11, 2022

45. Gosh, M., Barman, A., Meikap, A. K., De, S. K., & Chatterjee, S. (1999). Hopping transport in HCl doped conducting polyaniline. *Physics Letters A*, *260*(1-2), 138-148..

46. Bisquert, J., Garcia-Belmonte, G., Bueno, P., Longo, E., & Bulhoes, L. O. S. (1998). Impedance of constant phase element (CPE)-blocked diffusion in film electrodes. *Journal of Electroanalytical Chemistry*, *452*(2), 229-234..

47. Patil, R., Roy, A. S., Anilkumar, K. R., Jadhav, K. M., & Ekhelikar, S. (2012). Dielectric relaxation and ac conductivity of polyaniline–zinc ferrite composite. *Composites Part B: Engineering*, *43*(8), 3406-3411..

48. Nabid, M. R., Golbabaee, M., Moghaddam, A. B., Dinarvand, R., & Sedghi, R. (2008). Polyaniline/TiO2 nanocomposite: enzymatic synthesis and electrochemical properties. *International journal of electrochemical science*, *3*(10), 1117-1126.

49. Li, J., Cui, M., Lai, Y., Zhang, Z., Lu, H., Fang, J., & Liu, Y. (2010). Investigation of polyaniline co-doped with Zn2+ and H+ as the electrode material for electrochemical supercapacitors. *Synthetic metals*, *160*(11-12), 1228-1233.

50. Li, J., Tang, X., Li, H., Yan, Y., & Zhang, Q. (2010). Synthesis and thermoelectric properties of hydrochloric acid-doped polyaniline. *Synthetic Metals*, *160*(11-12), 1153-1158..

51. Epstein, A. J., Ginder, J. M., Zuo, F., Bigelow, R. W., Woo, H. S., Tanner, D. B., ... & MacDiarmid, A. G. (1987). Insulator-to-metal transition in polyaniline. *Synthetic Metals*, *18*(1-3), 303-309..

ISSN PRINT 2319 1775 Online 2320 7876
Research paper
 UGC CARE Listed (Group -I) Journal Volume 11, Iss 11, 2022

52. Chatterjee, K., Ganguly, S., Kargupta, K., & Banerjee, D. (2011). Bismuth nitrate doped polyaniline–Characterization and properties for thermoelectric application. *Synthetic metals*, *161*(3-4), 275-279.